Hydrol. Earth Syst. Sci. Discuss., 11, 6441–6472, 2014
www.hydrol-earth-syst-sci-discuss.net/11/6441/2014/
doi:10.5194/hessd-11-6441-2014

Hydrology and Earth System Sciences
Open Access
Discussions

What causes cooling water temperature gradients in forested stream reaches?

G. Garner[1], I. A. Malcolm[2], J. P. Sadler[1], and D. M. Hannah[1]

[1]School of Geography, Earth and Environmental Sciences, University of Birmingham, Edgbaston, Birmingham, B15 2TT, UK
[2]Marine Scotland Science, Freshwater Laboratory, Faskally, Pitlochry, Perthshire, PH16 5LB, UK

Received: 21 May 2014 – Accepted: 27 May 2014 – Published: 17 June 2014

Correspondence to: G. Garner (g.garner@bham.ac.uk)

Published by Copernicus Publications on behalf of the European Geosciences Union.

Abstract

Previous studies have suggested that shading by riparian vegetation may reduce maximum water temperature and provide refugia for temperature sensitive aquatic organisms. Longitudinal cooling gradients have been observed during the daytime for stream reaches shaded by coniferous trees downstream of clear cuts, or deciduous woodland downstream of open moorland. However, little is known about the energy exchange processes that drive such gradients, especially in semi-natural woodland contexts, and in the absence of potentially confounding cool groundwater inflows. To address this gap, this study quantified and modelled variability in stream temperature and heat fluxes along an upland reach of the Girnock Burn (a tributary of the Aberdeenshire Dee, Scotland) where riparian landuse transitions from open moorland to semi-natural forest. Observations were made along a 1050 m reach using a spatially-distributed network of ten water temperature micro-loggers, three automatic weather stations and > 200 hemispherical photographs, which were used to estimate incoming solar radiation. These data parameterised a high-resolution energy flux model, incorporating flow-routing, which predicted spatio-temporal variability in stream temperature. Variability in stream temperature was controlled largely by energy fluxes at the water column–atmosphere interface. Predominantly net energy gains occurred along the reach during daylight hours, and heat exchange across the bed-water column interface accounted for < 1 % of the net energy budget. For periods when daytime net radiation gains were high (under clear skies), differences between water temperature observations decreased in the streamwise direction; a maximum difference of 2.5 °C was observed between the upstream reach boundary and 1050 m downstream. Furthermore, daily maximum water temperature at 1050 m downstream was ≤ 1 °C cooler than at the upstream reach boundary and lagged the occurrence of daily maximum water temperature upstream by > 1 h. Temperature gradients were not generated by cooling of stream water, but rather by a combination of reduced rates of heating in the woodland reach and advection of cooler (overnight and early morning)

HESSD
11, 6441–6472, 2014

water from the upstream moorland catchment. Longitudinal thermal gradients were indistinct at night and on days when net radiation gains were low (under over-cast skies), thus when changes in net energy gains or losses did not vary significantly in space and time, and heat advected into the reach was reasonably consistent. The findings of the study and the modelling approach employed are useful tools for assessing optimal planting strategies for mitigating against ecologically damaging stream temperature maxima.

1 Introduction

River temperature dynamics are of increasing interest to the scientific community, environment managers and regulators (Hannah et al., 2008), particularly given the contexts of a changing climate (e.g. van Vliet et al., 2011; Beechie et al., 2013) and associated profound consequences of high water temperature for aquatic ecosystems (Poole and Berman, 2001; Caissie, 2006; Webb et al., 2008; Wilby et al., 2010; Leach et al., 2012). Numerous studies have demonstrated that the presence of riparian woodland can decrease diurnal variability, mean and maximum stream temperatures (e.g. Malcolm et al., 2008; Brown et al., 2010; Imholt et al., 2012; Garner et al., 2014), or conversely that forest removal results in temperature increases (e.g. Macdonald et al., 2003; Rutherford et al., 2004; Danehy et al., 2005; Moore et al., 2005; Gomi et al., 2006). Consequently, there is substantial interest from researchers and stream managers in the potential of riparian vegetation cover to mitigate against climate change impacts (e.g. The River Dee Trust; Upper Dee Planting Scheme, 2011), especially in relation to thermal maxima.

Several studies have documented daytime cooling gradients (decreases in temperature in a streamwise direction measured at a single point in time) beneath forest canopies downstream of open (no trees) landuse, although the magnitude of reported cooling effects varied between studies (e.g. Brown, 1971; Rutherford et al., 1997; McGurck, 1989; Keith et al., 1998; Zwieniecki and Newton, 1999; Torgerson

HESSD
11, 6441–6472, 2014

et al., 1999; Story et al., 2003). For example, McGurck (1989), Keith et al. (1998) and Story et al. (2003) observed gradients of between 4.0 and 9.2 °C km^{-1}. However, little is known about the energy exchange processes that generate this apparent cooling effect (Story et al., 2003). Studies conducted by Brown (1971) and Story et al. (2003) observed net energy gains to the water column measured predominantly across the air-water column interface. The presence of net energy gain conditions lead both Brown (1971) and Storey et al. (2003) to attribute the generation of cooling gradients to reach-scale groundwater inputs that were underestimated by point-scale energy exchange measurements (e.g. Brown, 1971; Story et al., 2003; Moore et al., 2005; Leach and Moore, 2011; Garner et al., 2014). Cooling gradients have also been observed in forested reaches downstream of open landuse in which groundwater inputs and hyporheic exchange are known to be minimal (e.g. Malcolm et al., 2004; Imholt et al., 2010, 2012). However, a conceptualisation of the processes driving observed patterns of cooling in forested reaches without groundwater inputs is lacking; this is essential if stream managers are to plan future riparian planting strategies that maximise benefits at minimal cost.

This study aims to quantify and model spatio-temporal variability in stream water temperature and heat fluxes for an upland reach of the Girnock Burn (a tributary of the Aberdeenshire Dee, Scotland) where riparian landuse transitions from open moorland to semi-natural forest and stream temperature variability is driven largely by fluxes at the water column–atmosphere interface (i.e. not confounded by groundwater–surface water interactions). The specific objectives are:

1. To quantify the magnitude of longitudinal water temperature gradients within the reach and identify the meteorological conditions under which the strongest and weakest gradients occur.

2. To explore the effect of changing riparian vegetation density on heat fluxes within the reach.

HESSD
11, 6441–6472, 2014

3. To understand, using a simple flow routing model in conjunction with a Lagrangian water temperature model, how water temperature changes as it travels through the forested reach and attribute this to underlying processes.

2 Study area

A 1050 m study reach with no tributary inputs was established within Glen Girnock, an upland basin that drains into the Aberdeenshire Dee, northeast Scotland. Upstream of the reach ($\sim 24\,km^2$), landuse is dominated by heather (*Calluna*) moorland. Within the reach landuse transitions from open moorland to semi-natural forest composed of birch (*Betula*), Scots pine (*Pinus*), alder (*Alnus*) and willow (*Salix*) (Imholt et al., 2012).

Full details of the Girnock catchment characteristics are found in Tetzlaff et al. (2007). In brief, soils are composed primarily of peaty podsols with a lesser coverage of peaty gleys. Granite at higher elevations and schists at lower elevations dominate the geology, both of which have relatively impermeable aquifer properties. Groundwater movement is mainly by fracture flow (Tetzlaff et al., 2007). The rivedbed is composed of a series of gravel–cobble riffles (Hannah et al., 2008). Previous work in the catchment suggests highly heterogeneous but spatially constrained groundwater discharge, with no significant groundwater inputs within the study reach (Malcolm et al., 2005). Hyporheic conditions within the study reach are characterised by very slight downwelling surface water (Malcolm et al., 2005). Thus contributions to streamflow are derived predominantly from surface water, and heat exchange within the reach was anticipated to be dominated predominantly by fluxes at the water column–atmosphere interface. The Girnock Burn flows in a mainly northerly direction and so experiences no significant changes in aspect that may influence solar radiation receipt along the reach (Fig. 1). Maximum and minimum elevations of the reach are respectively 280 and 255 m (Fig. 1). Mean river width was 9.5 m during the study period.

HESSD
11, 6441–6472, 2014

3 Methods

3.1 Experimental design

Ten water temperature loggers were deployed throughout a 1050 m reach of the Girnock where riparian landuse transitions from open moorland to semi-natural forest (Fig. 1), and in which previous studies have identified measurable changes in stream temperature (e.g. Malcolm et al., 2004, 2008; Imholt et al., 2010, 2012). Three automatic weather stations (AWSs) were deployed along the reach to estimate spatio-temporal variability in energy fluxes: one in open moorland (AWS_{open}) and two in semi-natural forest (AWS_{FUS} followed by AWS_{FDS}). The number and location of AWSs was limited by logistical and financial constraints. However, in excess of 200 hemispherical photographs were taken at 5 m intervals along the reach so that solar radiation measured at the open site AWS could be re-scaled to estimate radiative fluxes at a high spatial resolution. For locations where hemispherical images were taken, turbulent (i.e. latent and sensible heat) and bed heat fluxes were estimated by linearly interpolating between values at the two nearest AWSs. High resolution information on energy fluxes and stream temperature was combined with a flow-routing model to provide process-based understanding of spatio-temporal variability in stream temperature.

3.2 Data collection

Field data were collected between October 2011 and July 2013. A seven-day period comprising of 1–7 July 2013 was chosen to meet the aims of the present study because high air temperatures (i.e. > average air temperatures for this week in the preceding ten years) and extremely low flows (i.e. < average minimum flows for this week in the preceding ten years) occurred (Fig. 2). High energy gains occurred on six days and relatively low energy gains occurred on one day. These data allowed assessment of: (1) potential mitigation of high temperatures by semi-natural forest under a "worst

HESSD
11, 6441–6472, 2014

case scenario" of high energy gains and low flows; and (2) the influence of contrasting prevailing meteorological conditions on longitudinal water temperature patterns.

3.2.1 Stream temperature measurements

Stream temperature measurements were made at 15 min intervals across a spatially-distributed network of ten water temperature TinyTag Aquatic 2 micro-loggers and three Campbell 107 thermistors connected to AWSs at 0 (AWS_{open}), 190, 315, 460, 565, 630, 685 (AWS_{FUS}), 760, 815, 865, 940, 1015 and 1050 (AWS_{FDS}) m downstream of the upstream reach boundary (Fig. 1). The sensors were cross-calibrated (Hannah et al., 2009) prior to installation and showed good agreement (i.e. $< \pm 0.1\,^{\circ}C$). Within the reach, sensors were housed in white plastic PVC tubes to shield them from direct solar radiation.

3.2.2 Hydrology and stream geometry

Flow accretion surveys (following the velocity-area method) were conducted at 200 m intervals along the reach to assess net flow gains and losses between the channel and subsurface (Leach and Moore, 2011). No significant gains or losses were observed, with differences between gaugings consistently within ±10 % of each other (i.e. within velocity–area measurement uncertainty; Leach and Moore, 2011). These gaugings upheld the assumption that groundwater gains and losses along the reach were negligible.

A Scottish Environmental Protection Agency (SEPA) gauging station at Littlemill (Fig. 1) provided discharge data at 15 min intervals. The discharge- mean velocity function for Littlemill presented in Tetzlaff et al. (2005) was used to calculate water velocity and thus drive the flow-routing model. Good correspondence was observed between velocities measured during flow accretion surveys and those calculated from discharge at Littlemill. Stream surface width was measured at 50 m intervals along the reach.

HESSD
11, 6441–6472, 2014

3.2.3 Micrometeorological measurements

Three automatic weather stations (AWSs) were installed within the reach (Fig. 1). The instruments deployed on AWSs are detailed in Hannah et al. (2008). All sensors were cross-calibrated prior to installation and correction factors applied, if required. Hydrometeorological variables measured included air temperature, relative humidity, wind speed, shortwave radiation and bed heat flux. The sensors sampled at 10 s intervals, with averages logged every 15 min.

3.2.4 Hemispherical images

Hemispherical images were taken at 5 m intervals along the stream centreline using a Canon EOS-10D 6.3 megapixel digital camera with Sigma 8 mm fisheye lens. Prior to taking each image the camera was orientated to north and levelled ~ 20 cm above the stream surface (Leach and Moore, 2010).

3.3 Estimation of stream energy balance components

3.3.1 Net energy

Net energy ($W\,m^{-2}$) available to heat or cool the water column was calculated as:

$$Q_n = Q^* + Q_e + Q_h + Q_{bhf} \quad (1)$$

Where Q_n is net energy, Q^* is net radiation, Q_e is latent heat and Q_h is sensible heat (all $W\,m^{-2}$). Heat from fluid friction was assumed to be negligible (see Garner et al., 2014) and was therefore omitted. Herein, energy fluxes are considered to be positive (negative) when directed toward (away from) the water column.

HESSD
11, 6441–6472, 2014

3.3.2 Net radiation

A deterministic model developed by Moore et al. (2005) and evaluated by Leach and Moore (2010) was used to compute net radiation (Q^*) at the location of each hemispherical image. At each location, the model was expressed as:

$$Q^* = (1-\alpha)[D(t)g(t) + S(t)f_v] + \left[f_v\varepsilon_a + (1-f_v)\varepsilon_{vt}\right]\sigma(T_a + 273.2)^4 - \varepsilon_w\sigma(T_w + 273.2)^4 \quad (2)$$

Where α is the stream albedo, $D(t)$ is the direct component of incident solar radiation at time t ($W\,m^{-2}$), $g(t)$ is the canopy gap fraction at the position of the sun in the sky at time t, $S(t)$ is the diffuse component of solar radiation, f_v is the sky view factor, ε_a, ε_{vt} and ε_w are respectively the emissivity of the temperatures of the air, vegetation and water (°C), σ is the Stefan–Boltzmann constant ($5.67\times10^{-8}\,W\,m^{-2}\,K^{-4}$), and T_a and T_w are respectively air and water temperature (°C).

Values for atmospheric emissivity were calculated for clear-sky day and night conditions using the equation presented in Prata (1996; used also by Leach and Moore, 2010) and were subsequently adjusted for cloud cover using equations in Leach and Moore (2010). The emissivity and albedo were taken, respectively, to be 0.95 and 0.05 for water, and 0.97 and 0.03 for vegetation (Moore et al., 2005).

Gap fractions (g^*) were computed as a function of solar zenith angle (θ) and solar azimuth (ψ), $g^*(\theta\psi)$, which were derived from analysis of the hemispherical images with Gap Light Analyser software (Frazer et al., 1999). Using equations in Iqbal (1983), the solar zenith and azimuth angles were computed as a function of time, t, so that the canopy gap at the location of the sun's disk could be derived from $g^*(\theta\psi)$ as a function of time, $g(t)$. View factor was computed as:

$$f_v = \frac{1}{\pi}\int_0^{2\pi}\int_0^{\pi/2} g^*(\theta,\psi)\cos\theta\sin\theta\cdot d\theta\cdot d\psi \quad (3)$$

HESSD
11, 6441–6472, 2014

The double integral was approximated by summation using an interval of 5° for both solar zenith and azimuth angles (after Leach and Moore, 2010). Solar radiation measurements made at AWS_{open} were used as input to the radiation models.

3.3.3 Latent and sensible heat fluxes

Latent heat was estimated using a Penman-style equation (after Webb and Zhang, 1997) to compute heat lost by evaporation or gain by condensation (Eq. 4).

$$Q_e = 285.9(0.132 + 0.143 \cdot U)(e_a - e_w) \quad (4)$$

Where U is wind speed ($m\,s^{-1}$) and e_a and e_w are vapour pressures of air and water (kPa), respectively.

Vapour pressure of water (e_w) was assumed to be equal to $e_{sat}(T_w)$. Vapour pressure of air was calculated using Eq. (6).

$$e_{sat}(T) = 0.611 \cdot \exp\left[\frac{2.5 \times 10^6}{461} \cdot \left(\frac{1}{273.2} - \frac{1}{T}\right)\right] \quad (5)$$

$$e_a = \frac{RH}{100} e_{sat}(T_a) \quad (6)$$

Sensible heat ($W\,m^{-2}$) was calculated as a function of Q_e (Eq. 3) and Bowen ratio (β) (Eq. 8), where P is air pressure (kPa).

$$Q_h = Q_e \cdot \beta \quad (7)$$

$$\beta = 0.66 \cdot \left(\frac{P}{1000}\right) \cdot [(T_w - T_a)/(e_a - e_w)] \quad (8)$$

HESSD
11, 6441–6472, 2014

3.4 Modelling approaches

3.4.1 Statistical models

Spatial (and temporal) variability in canopy density (and net energy flux) was extremely high. Therefore, generalised additive models (GAMs; Hastie and Tibshirani, 1986) were used to provide continuous smoothed estimates of the variability in each dataset so that broad patterns in space and time could be identified.

The GAM fitted to canopy density provided a continuous smoothed estimate of the spatial variability in density from discrete (5 m interval) point measurements determined from Gap Light Analyser outputs. Canopy density was calculated as the percentage of pixels representative of vegetation in each hemispherical image; this percentage was modelled as a smoothed function of distance downstream (i.e. from AWS_{open}).

The second GAM provided a continuous smoothed estimate of the spatio-temporal variability in net energy flux estimated at 5 m intervals from the sum of scaled radiative flux (see Sect. 3.3.2), and turbulent and bed heat fluxes determined by linear interpolation between the two nearest AWSs. Specifically, net energy was modelled as smoothed functions of: (i) time of day, (ii) day of year, and (iii) distance downstream.

GAMs were fitted in the MGCV package (Wood, 2006; version 1.7–13) for R (Version 3.0.2, R Group for Statistical Computing, 2013). Degrees of freedom were estimated by MGCV but limited (gamma = 1.4) to prevent over-fitting (Wood, 2006). The inclusion of three smoothed terms in the net energy GAM was validated by fitting models using each possible combination of terms and comparing AIC (Akaike information criterion; Burnham and Anderson, 2002) score (a measure of model performance that balances fit and parsimony) between models. The GAM with the three proposed smoothed terms (above) yielded the lowest AIC score (i.e. more than two units lower than for each of the simpler models) and was thus chosen as the optimum model to be fitted to net energy.

HESSD
11, 6441–6472, 2014

3.4.2 Flow routing model

A flow routing model was used to predict the time taken by water parcels to travel through the reach. The model was based on the discharge- mean velocity function (Tetzlaff et al., 2005) and predicted the distance travelled by water parcels at 15 min intervals. In combination with the dataset of spatio-temporally distributed water temperature observations, the model also identified the temperature of distinct water volumes at 15 min intervals.

The model released water (i) from AWS_{open} every hour on each day of the study period. For each parcel of water, the time taken (Δt) for it to travel between its current position (x) at time t and the next temperature sensor in the downstream direction ($x+1$) was calculated as the quotient of the distance between x and $x+1$ and its velocity at x. The velocity of the parcel was allowed to change at each timestep. The temperature of the parcel at location $x+1$ was assumed to be the temperature recorded by the sensor located at $x+1$ at time $t+\Delta t$ to the nearest 15 min.

3.4.3 Lagrangian water temperature model

The Lagrangian modelling approach (after Rutherford et al., 2004; Leach and Moore, 2011; MacDonald et al., 2014) divided the reach into a series of segments bounded by nodes (indexed by i). For each time step, Δ_{900} (s), a water parcel (indexed by j) was released from the upstream boundary; its initial temperature was an observed value. As the water parcel travelled downstream from i towards $i+1$ the model computed the heat exchange and the net change in stream temperature over the segment (Eq. 9).

$$\frac{\mathrm{d}T_{\mathrm{w}}}{\mathrm{d}x} = \frac{W_{(i)}\left[Q^{*}_{(i,t)} + Q_{\mathrm{h}(i,t)} + Q_{\mathrm{e}(i,t)} + Q_{\mathrm{bhf}(i,t)}\right]}{C \cdot F_{(i,t)}} \tag{10}$$

Where $W_{(i)}$ is the mean width of the stream surface (m), $Q^{*}_{(i,t)}$, $Q_{\mathrm{e}(i,t)}$, $Q_{\mathrm{h}(i,t)}$ and $Q_{\mathrm{bhf}(i,t)}$ are the net radiative, latent, sensible and bed heat fluxes at node i and time t (W m^{-2}).

HESSD
11, 6441–6472, 2014

C is the specific heat capacity of water (4.18×10^6 J m^{-3} °C^{-1}) and $F_{(i,t)}$ is the discharge (m^3 s^{-1}; scaled by catchment area) at node i and time t.

The temperature of each water parcel was modelled at 1 m intervals along the reach by solving Eq. (9) numerically in the deSolve package (Soetaert et al., 2010) for R (Version 3.0.2, R Group for Statistical Computing, 2013).

Incident solar radiation was modelled at 5 m intervals (see Sect. 3.3.2); values at 1 m intervals were interpolated linearly. Emitted longwave radiation, latent and sensible heat fluxes were dependent on water temperature. Therefore, these fluxes were calculated at each time step within Eq. (9) using values for air temperature, humidity and wind speed calculated by interpolation linearly between the two AWSs nearest to the node.

4 Results

Results are presented in four sections: (1) prevailing weather conditions; (2) observed spatio-temporal water temperature patterns; (3) riparian canopy density and net energy flux patterns, and (4) modelled spatio-temporal water temperature patterns.

4.1 Prevailing hydrological and weather conditions

Stream discharge measured at Littlemill was very low, reasonably stable, and exhibited no sudden changes throughout the study period (Fig. 2). The 1st, 3rd, 4th, 5th, 6th and 7th days of the study period were characterised by high net energy gains to the water column during daylight hours, driven by clear-skies and consequently high solar radiation receipt (Fig. 2). On the 2nd day, net energy gains were markedly lower, due to overcast skies and associated low solar radiation receipt (Fig. 2). This data window permitted consideration of the influence of contrasting energy gain conditions (i.e. low vs. high net energy gain) on the spatio-temporal variability of water temperature and energy flux.

HESSD
11, 6441–6472, 2014

4.2 Observed spatio-temporal water temperature patterns

Minimum daily water temperature was the same at both AWS_{open} and AWS_{FDS} (9.8 °C) but maximum temperature was higher at AWS_{open} than at AWS_{FDS}, with observed temperatures of 23.0 and 22.0 °C (both occurring on the 6th day), respectively. Minimum temperatures occurred synchronously across all locations. Maximum temperatures at AWS_{FDS} lagged those at AWS_{open} by between 1 and 1.75 h on all days except the 2nd (which was overcast, and the water column received lower solar receipt), when maximum temperatures occurred synchronously across all locations.

Longitudinal gradients in instantaneous water temperature measurements (at a particular point in time across the entire reach) were observed during daylight hours on each day of the study period. Instantaneous water temperature was greatest at AWS_{open} and decreased downstream towards AWS_{FDS}. Large daily temperature amplitudes (Fig. 3a) and distinct downstream gradients of > 1 °C (Fig. 3b) were observed on the 1st, 3rd, 4th, 5th, 6th and 7th days between 11:00 and 16:00 GMT. The greatest instantaneous temperature gradient was 2.5 °C in magnitude, observed on the 6th day at 12:00 GMT (Fig. 3b and d). On the 2nd day, the diurnal water temperature cycle was greatly reduced and longitudinal water temperature gradients were small (Fig. 3c and d) with the greatest gradient (0.6 °C) observed at 08:00 GMT, and smaller gradients (< 0.2 °C i.e. below measurement accuracy of the sensors) observed between 11:00 and 15:00 GMT.

Overnight, longitudinal gradients were reversed (cf. daylight hours); instantaneous water temperature was lowest at AWS_{open} and increased downstream towards AWS_{FDS} (Fig. 3b). However, the difference in temperature between these two sites was consistently < 0.5 °C in magnitude.

HESSD
11, 6441–6472, 2014

4.3 Riparian canopy density and energy flux patterns

Between AWS_{open} (0 m) and 400 m patchy forest cover (Fig. 4a and b) generated canopy density ranging from 0.0 to 70.3 % (Fig. 5a). Between 400 m and 1050 m (AWS_{FDS}) continuous riparian forest of variable density (Fig. 4c and d) produced typically lower, but more variable gap fractions ranging from 22.5 to 92 % (Fig. 5a). The forest canopy was densest between 400 and 800 m and decreased in density between 800 and 1050 m Fig. 5a).

The spatial variability in net energy corresponded broadly inversely to canopy density. Net energy gains during daylight hours decreased gradually from AWS_{open} to 400 m before declining sharply between 400 and 800 m. Between 800 and 1050 m (AWS_{FDS}), net energy flux increased markedly. Strong diurnal signals and distinct spatial patterns were observed during daylight hours on the 1st, 3rd, 4th, 5th, 6th and 7th days, with spatial patterns especially clear around solar noon (Fig. 5b). On the 2nd day, the spatial and temporal variability of net energy fluxes was much subdued. Around solar noon on the 2nd day, net energy flux was slightly lower at 800 m but differences within the reach were otherwise indistinguishable (Fig. 5c), driven by smaller differences (relative to clear sky conditions) in solar radiation gain between open and forested sites (Fig. 2c–e).

Nocturnally, small and temporally consistent differences in net energy occurred within the reach (Fig. 5). Net energy losses were greatest at AWS_{open} and declined up until 400 m before stabilising and increasing again between 800 m and 1050 m, yet spatial variability was reduced drastically in comparison to daytime conditions on the 1st, and 3rd through 7th days.

4.4 Modelled spatio-temporal water temperature patterns

The flow routing model was evaluated by predicting the change in temperature of water parcels (using the water temperature model). Observed temperature changes over the reach were compared with those predicted for water leaving AWS_{open} (0 m, the

HESSD
11, 6441–6472, 2014

upstream boundary of the reach) at 06:00, 07:00, 08:00, and 09:00 GMT (i.e. when the greatest temperature increases were observed). Predictions of downstream water temperature change were typically good (Fig. 6).

Using the flow routing model, the time taken for water to travel 1050 m through the reac h from AWS_{open} to AWS_{FDS} averaged 7.5 h. Typically, water travelling from the upstream boundary of the reach between 01:00 and 12:00 GMT warmed as it travelled through the reach while water beginning its journey through the reach between 13:00 and 00:00v cooled (Fig. 7).

On the 1st, 3rd, 4th, 5th, 6th and 7th days water warmed between 4.2 and 6.9 °C while travelling through the reach; but, at the time of arrival at AWS_{FDS}, it was cooler than the water temperature observed at AWS_{open} at the same time (Fig. 7a). For example, on the 6th day water leaving AWS_{open} at 08:00 GMT was 14.3 °C. This water passed through the reach and arrived at AWS_{FDS} at 15:30 GMT, by which time its temperature had risen to 19.9 °C. The water leaving AWSopen at 15:30 GMT had a temperature of 21.4 °C (Fig. 7a and c). Thus at 15:30 GMT, the water at AWS_{FDS} was 1.5 °C cooler than that at AWS_{open}.

Distinct instantaneous cooling gradients were not observed on the 2nd day, when water warmed < 1.5 °C while travelling through the reach. The water travelling from AWS_{open} on day two at 07:00 GMT had a temperature of 10.4 °C and reached AWS_{FDS} at 14:15 GMT attaining a temperature of 11.8 °C. Water travelling downstream from AWS_{open} at 14:15 GMT also had a temperature of 11.8 °C and thus no cooling gradient was observed (Fig. 7b).

5 Discussion

This study has quantified longitudinal water temperature patterns in a stream reach where landuse transitions from open moorland to semi-natural forest. Furthermore, the riparian landuse controls plus associated energy exchange and water transport processes that generate water temperature patterns have been identified. Significant

HESSD
11, 6441–6472, 2014

groundwater inflows do not occur within the reach and thus energy exchange was dominated by fluxes at the air-water column interface, allowing clearer conceptual understanding of the processes of longitudinal stream water cooling gradients under forest canopies. The following discussion identifies the key drivers and processes, and their space-time dynamics.

5.1 Micrometeorological and landuse controls on energy exchange and water temperature

During daylight hours net energy gains modelled at 5 m resolution throughout the reach, corroborating the observations of Brown et al. (1971) and Story et al. (2003) for shaded streams downstream of clearings. Distinctive longitudinal patterns in net energy within the reach were observed on clear skies days when solar radiation, and net energy gains were greatest; whereas net energy varied little within the reach on overcast days indicating that meteorological conditions were a first-order control on patterns of net energy flux (Rutherford et al., 1997, 2004). The density of the semi-natural riparian forest canopy was a second order control on net energy flux. On clear-sky days, net energy gain was greatest where trees were absent (Moore et al., 2005) or the canopy was sparse, and least where the canopy was densest (Leach and Moore, 2010), owing to the canopy providing shading from solar radiation (Beschta and Taylor, 1988; Macdonald et al., 2003; Malcolm et al., 2004; Moore et al., 2005; Hannah et al., 2008; Imholt et al., 2010, 2012).

Contrasting meteorological conditions, and thus net energy gain conditions within the study period drove differences in the timing and magnitude of water temperature dynamics (Malcolm et al., 2004) and gradients observed within the reach. On overcast days, within-reach differences in the magnitude (Johnson and Jones, 2000) and timing of maximum daily temperatures, and longitudinal water temperature gradients were indistinguishable. However, on clear sky days, maximum daily temperatures decreased between the upstream and downstream reach boundary by up to 1 °C, locations further downstream experienced maximum temperatures later in the day and instantaneous

HESSD
11, 6441–6472, 2014

cooling gradients of up to 2.5 °C (equivalent to 2.4 °C km^{-1}) were observed. These decreases in temperature were much less than those observed by McGurck (1989), Keith et al. (1998) and Story et al. (2003) and, who observed instantaneous cooling gradients of between 4.0 and 9.2 °C km^{-1}. Variability in cooling gradients at and between sites may be attributed to differing climatic zones, prevailing weather conditions (Rutherford et al., 2004), riparian vegetation density and orientation, channel orientation and subsurface hydrology which all control the magnitude of energy exchange processes and consequently water temperature (Poole and Berman, 2001; Webb and Zhang, 1997).

5.2 Reconceptualisation of processes generating longitudinal water temperature gradients

The water temperature model reproduced downstream temperature patterns with a high level of accuracy using physically realistic parameters scaled from local micrometeorological and river flow measurements. This suggests that the energy balance was near closed. Previous studies (e.g. Story et al., 2003) have stated that cool groundwater inputs are necessary for longitudinal cooling gradients to occur. This study has demonstrated how cooling gradients can be produced in the absence of groundwater inputs in a shaded stream reach downstream of open landuse. It is now possible to conceptualise, for the first time, the processes that may generate spatio-temporal water temperature patterns on: (i) a clear sky day and (ii) an overcast sky day. On clear sky days, net energy fluxes increase reasonably consistently between sunrise and solar noon, driven by increasing solar radiation receipt. Consequently, the temperature of water crossing the upstream boundary and into the forest of the study reach between sunrise and solar noon increases continually (i.e. more heat is advected into the reach). On entering the forest, water temperature continues to increase but at a much reduced rate (Rutherford et al., 2004), as solar radiation and thus net energy are reduced considerably. Consequently, when net energy gains occur, water flowing

HESSD
11, 6441–6472, 2014

through the forest is consistently cooler than water travelling through the upper reach and moorland during the same time.

On overcast days, net energy gains increase little between sunrise and solar noon and differences in net energy gains between moorland and and forested sites are thus minimal. Therefore, the temperature of water crossing the upstream reach boundary changes little over the day (i.e. heat advected into the reach is reasonably constant) and water temperature changes at similar rates whether flowing through forest or moorland. Consequently, minor differences in water temperature are observed throughout the reach.

6 Conclusion

The findings of the study have a number of important implications for researchers and river managers who may wish to assess the potential to mitigate water temperature extremes using riparian shading (e.g. afforestation). The key finding is that water does not cool as it flows downstream under a semi-natural forest canopy. Instead, energy gains to the water column are reduced dramatically in comparison to open landuse, which reduces the rate at which water temperature increases. Thus, observed temperatures are controlled by a combination of lagged temperatures from upstream open reaches and lower rates of temperature increase within the forest. For reaches such as the Girnock Burn, where upstream landuse does not shade the channel, instantaneous longitudinal cooling gradients are generated when the temperature of water advected into the reach increases over the day, while temperature increases are minimal for the stream flowing underneath the forest canopy. This study was conducted under a "worst case" scenario of low flows and high energy gains; thus under these extreme conditions, cooler stream habitats are anticipated to be present under forest canopies during daylight hours, but warming of the water column upstream of the forest will control absolute water temperatures. Therefore shading headwater reaches, where water is not in dynamic equilibrium with the atmosphere (e.g. Erdinger et al.,

HESSD
11, 6441–6472, 2014

1968; Hrachowitz et al., 2010; Kelleher et al., 2012; Garner et al., 2013) and is thus cooler than the majority of locations lower in the basin (Poole and Berman, 2001), is anticipated to provide cool water habitats for temperature sensitive species and reduce temperatures further downstream.

Under future climates, surface energy balances are anticipated to change (Wild et al., 1997) and flow volume in catchments such as the Girnock, which have little storage and low groundwater residence time, is anticipated to be more variable/extreme (Cappel et al., 2013). The water temperature modelling approach used in this study allows researchers and stream managers to explore the effects of variable prevailing weather and hydraulic conditions on stream temperatures, and identify optimal locations for the generation of cooling gradients under different shading regimes under present and future climates. Future research should utilise tools such as those presented herein to understand the effects of climate, hydraulic conditions, channel orientation and shading scenarios on water temperature for which observational datasets are unavailable.

Author Contribution

I. A. Malcolm, G. Garner, and D. M. Hannah designed the study. G. Garner collected field data, wrote the flow-routing model and the water temperature model scripts, and performed the simulations. G. Garner prepared the manuscript with input from I. A. Malcolm, J. P. Sadler, and D. M. Hannah.

Acknowledgements. Grace Garner was funded by UK Natural Environment Research Council studentship (NE/1528226/1). Anne Anckorn is thanked for cartographic assistance. Jason Leach and Dan Moore generously shared their net radiation model script. Nigel Mottram is thanked for his advice on the water temperature model script. Marine Scotland Science Freshwater Laboratory staff provided valuable field and technical assistance, maintained and downloaded weather stations. SEPA provided discharge data. R was used for modelling and graphics.

HESSD
11, 6441–6472, 2014

References

Beechie, T., Imaki, H., Greene, J., Wade, A., Wu, H., Pess, G., Roni, P., Kimball, J., and Stanford, J., Kiffney, P., Mantua, N.: Restoring salmon habitat for a changing climate, River Res. Appl., 29, 939–960, 2013.

Beschta, R. L. and Taylor, R. L.: Stream temperature increases and land use in a forested Oregon watershed, Water Resour. Bull., 24, 19–25, 1988.

Brown, G. W., Swank, G. W., and Rothacher, J.: Water temperature in the Steamboat Drainage, USDA For. Serv. Res. Pap. PNW-119, 1971.

Brown, L. E., Cooper, L., Holden, J., and Ramchunder, S. J.: A comparison of stream water temperature regimes from open and afforested moorland, Yorkshire Dales, northern England, Hydrol. Process., 24, 3206–3218, 2010.

Burnham, K. P. and Anderson, D. R.: Model Selection and Multimodel Inference: a Practical Information-Theoretic Approach, Springer, New York, 480 pp., 2002.

Caissie, D.: The thermal regime of rivers: a review, Freshwater Biol., 51, 1389–1406, 2006.

Cappel, R., Tetzlaff, D., and Soulsby, C.: Will catchment characteristics moderate the projected effects of climate change on flow regimes in the Scottish Highlands?, Hydrol. Process., 27, 687–699, 2013.

Danehy, R. J., Colson, C. G., Parrett, K. B., and Duke, S. D.: Patterns and sources of thermal heterogeneity in small mountain streams within a forested setting, Forest Ecol. Manag., 208, 287–302, 2005.

Edinger, J. E., Duttweiler, D. W., and Geyer, J. C.: The response of water temperatures to meteorological conditions, Water Resour. Res., 4, 1137–1143, 1968.

Frazer, G. W., Canham, C. D., and Lertzman, K. P.: Gap Light Analyser (GLA), Version 2: Imaging Software to Extract Canopy Structure and Light Transmission Indices from True-Colour Fisheye Photographs, User's Manual and Program Documentation, Simon Fraser University and the Institute of Ecosystem Studies, Millbrook, NY, 36 pp., 1999.

Garner, G., Hannah, D. M., Sadler, J. P., and Orr, H. G.: River temperature regimes of England and Wales: spatial patterns, inter-annual variability and climatic sensitivity, Hydrol. Process., doi:10.1002/hyp.9992, in press, 2013.

Garner, G., Malcolm, I. A., Sadler, J. P., Millar, C. P., and Hannah, D. M.: Inter-annual variability in the effects of riparian woodland on micro-climate, energy exchanges and water

HESSD
11, 6441–6472, 2014

temperature of an upland Scottish stream, Hydrol. Process., doi:10.1002/hyp.10223, in press, 2014.
Gomi, T., Moore, R. D., and Dhakal, A. S.: Headwater stream temperature response to clear-cut harvesting with different riparian treatments coastal British Columbia Canada, Water Resour. Res., 42, W08437, doi:10.1029/2005WR004162, 2006.
Hannah, D. M., Malcolm, I. A., Soulsby, C., and Youngson, A. F.: A comparison of forest and moorland stream microclimate, heat exchanges and thermal dynamics, Hydrol. Process., 22, 919–940, 2008.
Hannah, D. M., Malcolm, I. A., and Bradley, C.: Seasonal hyporheic temperature dynamics over riffle bedforms, Hydrol. Process., 15, 2178–2194, 2009.
Hastie, T. J. and Tibshirani, R. J.: Generalized additive models, Stat. Sci., 1, 297–318, 1986.
Hrachowitz, M., Soulsby, C., Imholt, C., Malcolm, I. A., and Tetzlaff, D.: Thermal regimes in a large upland salmon river: a simple model to identify the influence of landscape controls and climate change on maximum temperatures, Hydrol. Process., 24, 3374–3391, 2010.
Imholt, C., Gibbins, C. N., Malcolm, I. A., Langan, S., Soulsby, C.: Influence of riparian tree cover on stream temperatures and the growth of the mayfly *Baetis rhodani* in an upland stream, Aquat. Ecol., 44, 669–678, 2010.
Imholt, C., Soulsby, C., Malcolm, I. A., Gibbins, C. N.: Influence of contrasting riparian forest cover on stream temperature dynamics in salmonid spawning and nursery streams, Ecohydrology, 6, 380–392, doi:10.1002/eco.1291, 2012.
Iqbal, M.: An Introduction to Solar Radiation, Academic Press, Toronto, 390 pp., 1983.
Johnson, S. L. and Jones, J. A.: Stream temperature responses to forest harvest and debris flows in Western Cascades Oregon, Can. J. Fish. Aquat. Sci., 57, 30–39, 2000.
Keith, R. M., Bjornn, T. C., Meehan, W. R., Hetrickm, J., and Brusvenn, M. A.: Response of juvenile salmonids to riparian and instream cover modifications in small streams flowing through second-growth forests of south-east Alaska, T. Am. Fish. Soc., 127, 899–907, 1998.
Kelleher, C., Wagener, T., Gooseff, M., McGlynn, B., McGuire, K., and Marshall, L.: Investigating controls on the thermal sensitivity of Pennsylvania streams, Hydrol. Process., 26, 771–785, 2012.
Leach, J. A. and Moore, R. D.: Above-stream microclimate and stream surface energy exchanges in a wildfire distributed zone, Hydrol. Process., 24, 2369–2381, 2010.
Leach, J. A. and Moore, R. D.: Stream temperature dynamics in two hydrogeomorphically distinct reaches, Hydrol. Process., 25, 679–690, 2011.

HESSD
11, 6441–6472, 2014

Leach, J. A., Moore, R. D., Hinch, S. G., and Gomi, T.: Estimation of logging-induced stream temperature changes and bioenergetic consequences for cutthroat trout in a coastal stream in British Columbia, Canada, Aquat. Sci., 74, 427–441, 2012.

Macdonald, J. S., MacIsaac, E. A., Heurer, H. E.: The effect of variable retention riparian buffer zones on water temperatures in small headwater streams in sub-boreal forest ecosystems of British Columbia, Can. J. Forest Res., 33, 303–316, 2003.

MacDonald, R. J., Boon, S., Byrne, J. M., Robinson, M. D., and Rasmussen, J. B.: Potential future climate effects on mountain hydrology, stream temperature and native salmon history, Can. J. Fish. Aquat. Sci., 71, 189–202, 2014.

Malcolm, I. A., Hannah, D. M., Donaghy, M. J., Soulsby, C., and Youngson, A. F.: The influence of riparian woodland on the spatial and temporal variability of stream water temperatures in an upland salmon stream, Hydrol. Earth Syst. Sci., 8, 449–459, doi:10.5194/hess-8-449-2004, 2004.

Malcolm, I. A., Soulsby, C., Youngson, A. F., and Hannah, D.M: Catchment scale controls on groundwater-surfacewater interactions in the hyporheic zone: implications for salmon embryo survival, River Res. Appl., 21, 977–989, 2005.

Malcolm, I. A., Soulsby, C., Hannah, D. M., Bacon, P. J., Youngson, A. F., and Tetzlaff, D.: The influence of riparian woodland on stream temperatures: implications for the performance of juvenile salmonids, Hydrol. Process., 22, 968–979, 2008.

McGurk, B. J.: Predicting stream temperature after riparian vegetation removal, in: Proceedings of the Californian Riparian Systems Conference: Protection, Management and Restoration for the 1990s, 22–24 September 1988, Davis, California, 157–164, 1988.

Moore, R. D., Sutherland, P., Gomi, T., and Dakal, A.: Thermal regime of a headwater stream within a clear-cut, coastal British Columbia, Hydrol. Process., 19, 2591–2608, 2005.

Prata, A. J.: A new long-wave formula for estimating downward clear-sky radiation at the surface, Q. J. Roy. Meteor. Soc., 122, 1127–1151, 1996.

Poole, G. C. and Berman, C. H.: An ecological perspective on in-stream temperature: natural heat dynamics and mechanisms human-caused thermal degradation, Environ. Manage., 27, 787–802, 2001.

R Core Team: R: a Language and Environment for Statistical Computing, R Foundation for Statistical Computing, Vienna, Austria, available at: http://www.R-project.org, last access: 27 May 2014, 2013.

HESSD
11, 6441–6472, 2014

Rutherford, J. C., Blackett, S., Blackett, C., Saito, L., and Davies-Colley, R. K.: Predicting the effects of shade on water temperature in small streams, New Zeal. J. Mar. Fresh., 31, 707–721, 1997.

Rutherford, J. C., Marsh, N. A., Davies, P. M., and Bunn, S. E.: Effects of patchy shade on stream water temperature: how quickly do small streams heat and cool?, Mar. Freshwater Res., 55, 737–748, 2004.

Story, A., Moore, R. D., and MacDonald, J. S.: Stream temperatures in two shaded reaches below cutblocks and logging roads: downstream cooling linked to subsurface hydrology, Can. J. Forest Res., 33, 1383–1396, 2003.

Soetaert, K., Petzoldt, T., Woodrow Setzer, R.: Solving differential equations in R: package deSolve, J. Stat. Softw., 33, 1–25, 2010.

Tetzlaff, D., Soulsby, C., Gibbins, C., Bacon, P. J., and Youngson, A. F.: An approach to assessing hydrological influences on feeding opportunities of juvenile Atlantic salmon (*Salmo salar*): a case study of two contrasting years in a small, nursery stream, Hydrobiologia, 549, 65–77, 2005.

Tetzlaff, D., Soulsby, C., Waldron, S., Malcolm, I. A., Bacon, P. J., Dunn, S. M., Lilly, A., and Youngson, A. F.: Conceptualisation of runoff processes using a geographical information system and tracers in a nested mesoscale catchment, Hydrol. Process., 21, 1289–1307, 2007.

Torgerson, C. E., Price, D. M., Li, H. W., and McIntosh, B. A.: Multiscale thermal refugia and stream habitat associations of chinook salmon in northeastern Oregon, Ecol. Appl., 9, 301–319, 1999.

Upper Dee riparian scheme, The River Dee Trust: available at: http://www.riverdee.org.uk/information/our_work.asp, last access: 5 June 2014, 2011.

van Vliet, M. T. H., Ludwig, F., Zwolsman, J. J. G., Weedon, G. P., and Kabat, P.: Global river temperatures and sensitivity to atmospheric warming and changes in river flow, Water Resour. Res., 47, W02544, doi:10.1029/2010WR009198, 2011.

Webb, B. W., Hannah, D. M., Moore, R. D., Brown, L. E., and Nobilis, F.: Recent advances in stream and river temperature research, Hydrol. Process., 22, 902–918, 2008.

Webb, B. W. and Zhang, Y.: Spatial and seasonal variability in the components of the river heat budget, Hydrol. Process., 11, 79–101, 1997.

Wilby, R. L., Orr, H. G., Watts, G., Battarbee, R. W., Berry, P. M., Chadd, R., Dugdale, S. J., Dunbar, M. J., Elliott, J. A., Extence, C., Hannah, D. M., Holmes, N., Johnson, A. C.,

HESSD
11, 6441–6472, 2014

Knights, B., Milner, N. J., Ormerod, S. J., Solomon, D., Timlett, R., Whitehead, J., and Wood, P. J.: Evidence needed to manage freshwater ecosystems in a changing climate: turning adaptation principles into practice, Sci. Total Environ., 408, 4150–4164, 2010.

Wild, M., Ohmura, A., and Cubasch, U.: GCM-simulated energy fluxes in climate change experiments, J. Climate, 10, 3093–3110, 1997.

Wood, S. N.: Generalized Additive Models: an Introduction with R, Boca Raton, Chapman and Hall/CRC, Boca Raton, 391 pp., 2006.

Yearlsey, J. R.: A semi-Lagrangian water temperature model for advection-dominated river systems, Water Resour. Res., 45, W12405, doi:10.1029/2008WR007629, 2009.

Zwieniecki, M. and Newton, M.: Influence of streamside cover and stream features on temperature trends in forested streams of western Oregon, West. J. Appl. For., 14, 106–112, 1999.

HESSD
11, 6441–6472, 2014

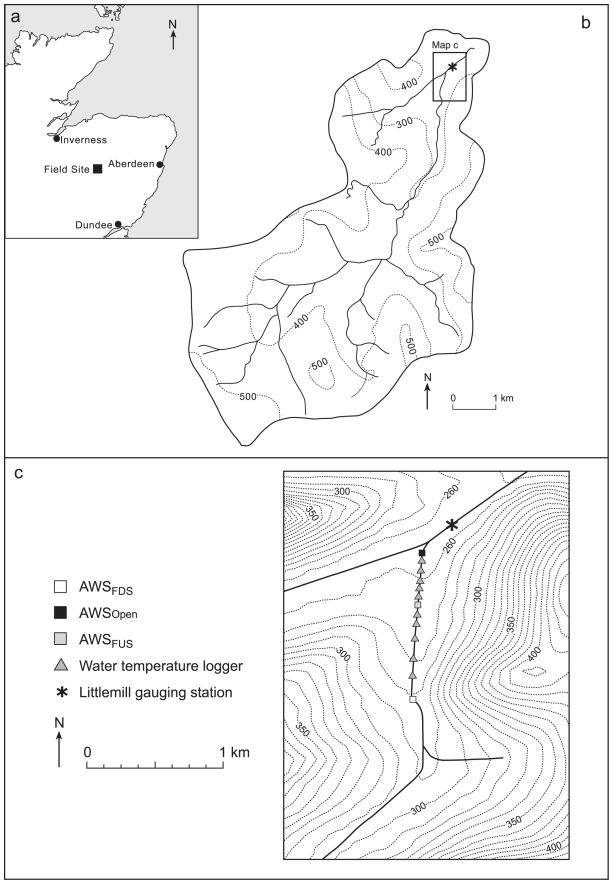

Figure 1. (a) Location map of the Girnock, **(b)** Girnock catchment, **(c)** locations of field data collection.

HESSD
11, 6441–6472, 2014

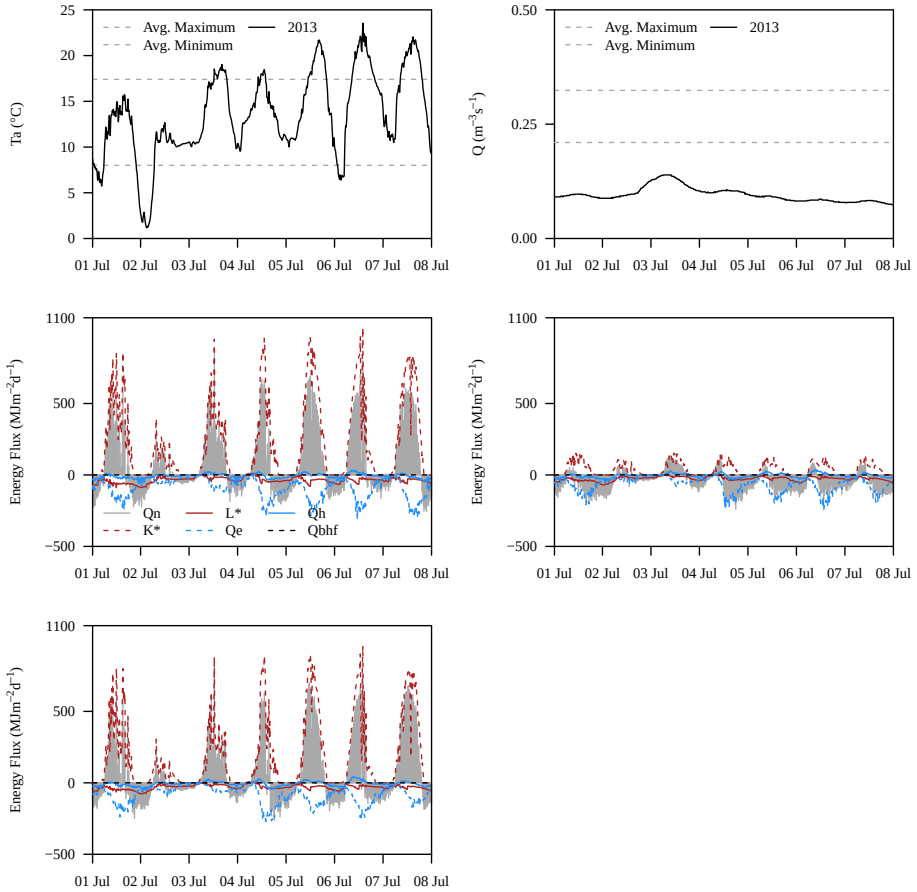

Figure 2. Study period **(a)** air temperature, **(b)** discharge, and energy fluxes at **(c)** AWS_{open}, **(d)** AWS_{FDS} and **(e)** AWS_{FUS}. Averages represent values for DOYs 183 to 189 in the 10 years preceding 2013.

HESSD
11, 6441–6472, 2014

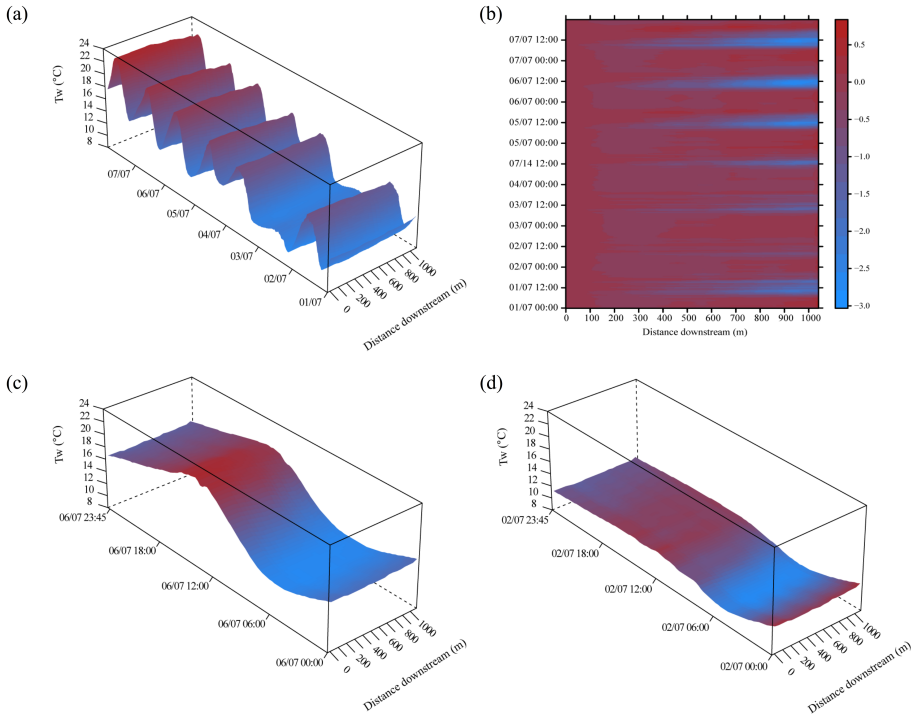

Figure 3. Spatial patterns in instantaneous water temperature measurements, **(a)** entire study period **(b)**, differences between AWS_{open} and each monitoring location, **(c)** 2nd day and **(d)** 6th day.

HESSD
11, 6441–6472, 2014

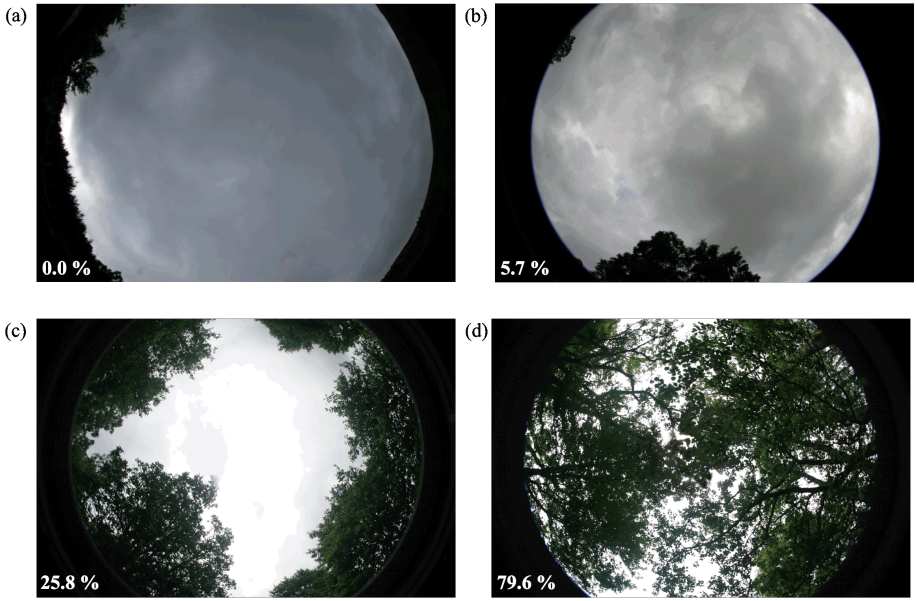

Figure 4. Hemispherical photographs representative of **(a)** clear sky view, **(b)** low density, patchy riparian forest **(c)** low density, continuous riparian forest, **(d)** high density, continuous riparian forest.

HESSD
11, 6441–6472, 2014

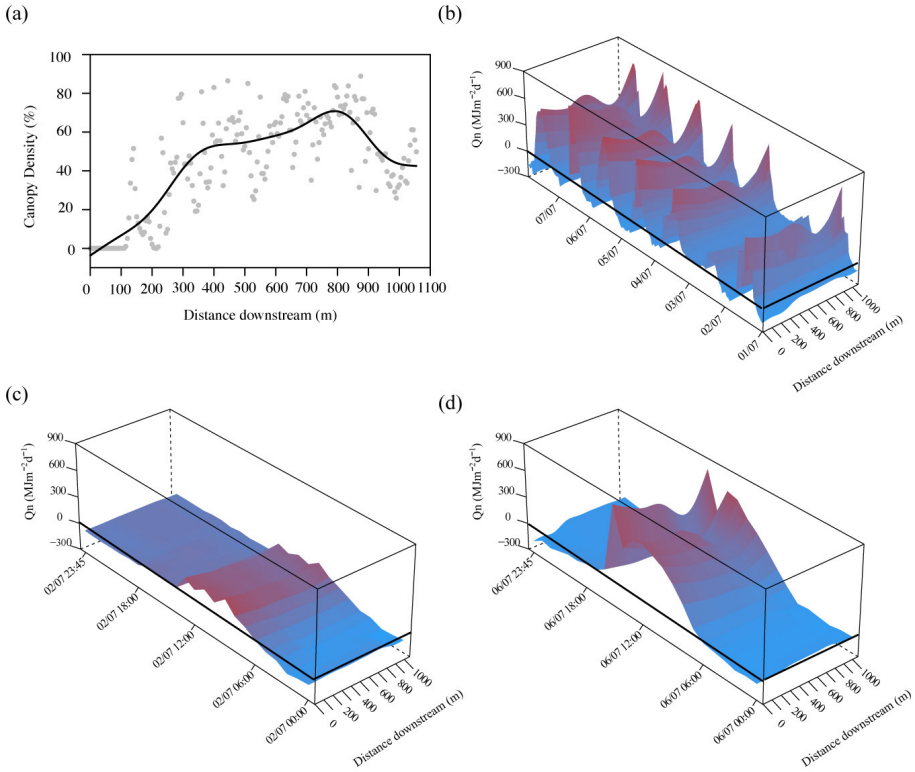

Figure 5. Spatial patterns within the reach in **(a)** total gap fractions and net energy flux **(b)** throughout the study period **(c)** on day two **(d)** on day six.

HESSD
11, 6441–6472, 2014

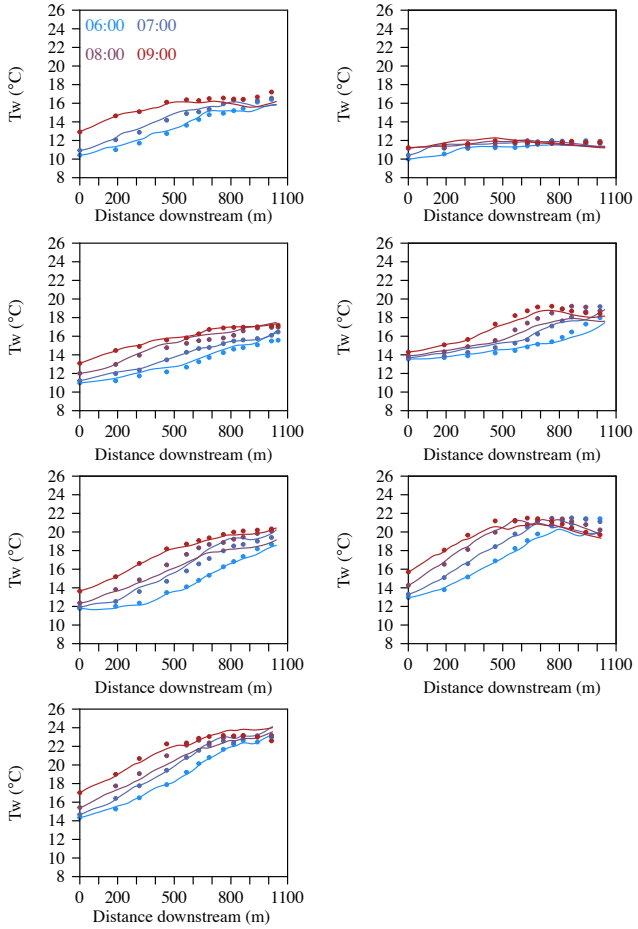

Figure 6. Modelled (solid lines) and observed (points) water temperature of water parcels released at 06:00, 07:00, 08:00 and 09:00 on **(a)** day one, **(b)** day two, **(c)** day three, **(d)** day four, **(e)** day five, **(f)** day six, **(f)** day seven.

HESSD
11, 6441–6472, 2014

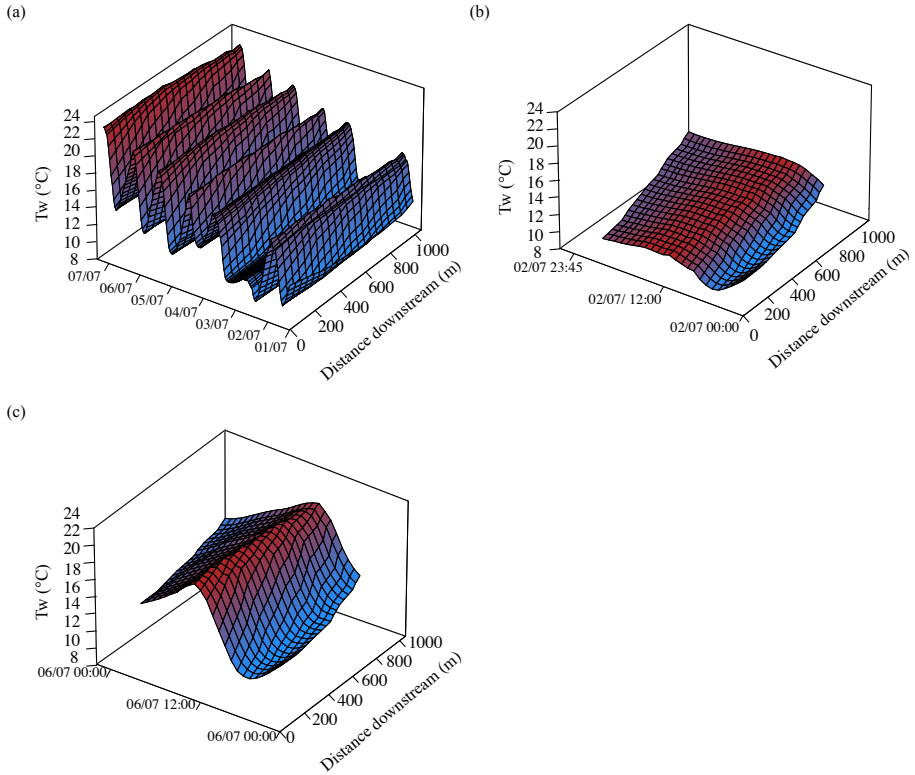

Figure 7. Temperature of water parcels (black lines on the date and time axis) routed through the reach from AWS_{open} at hourly intervals **(a)** on every day of the study period, **(b)** on day two, **(c)** on day six.

HESSD
11, 6441–6472, 2014